Emodin inhibits benzidine-enhanced survival and migration of upper urinary tract urothelial carcinoma cells by targeting the PKA/COX2 signaling pathway

YANYANG JIN[1], CHENGCAI WANG[1], KUN FENG[1], XIAOWEI WANG[2], MING TONG[1] and GUANGQUAN TONG[3]

[1]Department of Urology, The First Affiliated Hospital of Jinzhou Medical University, Jinzhou Medical University, Jinzhou, Liaoning 121001, P.R. China; [2]Department of Otorhinolaryngology, Head and Neck Surgery, The First Affiliated Hospital of Jinzhou Medical University, Jinzhou, Liaoning 121001, P.R. China; [3]Urological Oncology Surgery Ward 1, The First Affiliated Hospital of Jinzhou Medical University, Jinzhou, Liaoning 121001, P.R. China

Received May 21, 2024; Accepted August 16, 2024

DOI: 10.3892/ijo.2024.5691

Abstract. The carcinogenic effects of benzidine (BZ) on bladder cancer are well documented, but its potential for promoting upper urinary tract urothelial carcinoma (UTUC) remains unclear. The ability of emodin, a natural pharmaceutical compound, to prevent BZ-associated UTUC has not been previously explored. To the best of our knowledge, the present study is the first to reveal that BZ significantly enhanced the survival and migration of UTUC cell lines *in vitro*. Furthermore, *in vivo* experiments demonstrated that BZ promoted an increase in the size of subcutaneous tumors in nude mice. Further investigation revealed that BZ upregulated the expression of protein kinase A (PKA) and cyclooxygenase 2 (COX2), along with downstream matrix metalloproteinase 9 (MMP9) and vascular endothelial growth factor (VEGF), in UTUC cells. Moreover, BZ increased the levels of cyclic adenosine monophosphate (cAMP) and prostaglandin E2 (PGE2) in cell lysates. By contrast, emodin reduced the PKA and COX2 expression levels compared with the BZ-treated group. Similarly, the *in vivo* experiments demonstrated that emodin significantly inhibited tumor growth in BZ-pretreated nude mice, accompanied by reductions in the cAMP, PGE2, MMP9 and VEGF levels. These findings elucidated the role of BZ in promoting UTUC progression. Additionally, emodin has emerged as a novel inhibitor of BZ-induced UTUC development through PKA/COX2 inhibition, suggesting its potential as a natural therapeutic agent against BZ-associated UTUC.

Correspondence to: Dr Guangquan Tong, Urological Oncology Surgery Ward 1, The First Affiliated Hospital of Jinzhou Medical University, 18-2 Shuxiangmendi, Deshengli, Taihe, Jinzhou, Liaoning 121001, P.R. China
E-mail: yanyangjin789@163.com

Key words: benzidine, upper urinary tract urothelial carcinoma, emodin, protein kinase A, cyclooxygenase-2

Introduction

Benzidine (BZ) is a chemical compound used in the production of dyes, and its sulfate is used predominantly in industry (1). However, its carcinogenic properties have been well established, particularly in relation to bladder cancer (2). Historical observations dating back to the late 19th century, such as Rehn's findings in German aniline dye factories, first highlighted the link between BZ exposure and bladder cancer (2). Subsequent epidemiological studies and experimental validation further confirmed the carcinogenic nature of BZ, leading to its classification as a human carcinogen by the International Agency for Research on Cancer in 1987 (3). Despite its ban in commercial production, BZ continues to pose health risks as it is still found in various products, including hair dyes, paints and plastics (4).

Given the well-documented association between BZ exposure and bladder cancer, concerns about its potential role in promoting other urothelial carcinoma types, such as upper urinary tract urothelial carcinoma (UTUC), have increased. While urothelial carcinoma of the bladder is the most common urinary tract malignancy, accounting for 95% of cases, UTUC accounts for the remaining 5% of cases (5). However, whether BZ exposure contributes to the development of UTUC remains largely unexplored. Investigating the potential link between BZ and UTUC could provide valuable insights into the broader impact of BZ exposure on urothelial carcinogenesis and inform preventive measures to mitigate its adverse health effects.

Prostaglandin E2 (PGE2), a metabolite of arachidonic acid catalyzed by cyclooxygenase 2 (COX2), is known to promote tumor cell proliferation, angiogenesis, invasion and metastasis (6). A previous study has established a close link between the occurrence and development of UC and PGE2 (7). PGE2 exerts its effects by binding to four types of prostaglandin E receptors on the cell membrane, which regulate intracellular cyclic adenosine monophosphate (cAMP) levels, calcium ion concentrations and phosphatidylinositol activation (7). Upon activation of these receptors, the G protein undergoes a conformational change, leading to the separation of the

Gαs subunit from the Gβγ subunit, which subsequently activates adenylate cyclase to produce the second messenger cAMP (8). This molecule activates downstream regulatory elements such as protein kinase A (PKA), further promoting tumor proliferation and invasion (9). PKA expression may be linked to the invasive and metastatic properties of tumors, as its upregulation can activate metalloproteinases (MMPs), such as MMP9, which are essential for tumor infiltration (10). Additionally, PKA upregulation can increase the expression of several angiogenic factors, including vascular endothelial growth factor (VEGF) (11). In the context of UTUC, the COX2/PGE2/cAMP/PKA signaling pathway plays a critical role in tumor progression (12,13). Elevated levels of COX2 and its downstream products, such as PGE2, can enhance UTUC cell survival and migration. The subsequent increase in cAMP levels and activation of PKA further facilitates these processes, contributing to tumor growth and metastasis. Understanding the interplay between these molecular factors is crucial for developing targeted interventions to prevent or treat UTUC.

Rhubarb, a traditional Chinese herb, is renowned for its ability to enhance cardiovascular function (14,15). Emodin, a vital constituent present not only in rhubarb but also in various plants, such as Aloe vera, He Shou Wu and Tiger Balm (16), has garnered increasing attention for its notable antitumor, anti-inflammatory and antibacterial properties (14,15). Notably, a study has revealed that emodin suppresses VEGF transcription by targeting the transcription factors, nuclear receptor corepressor 2 and seryl-tRNA synthetase, thereby impeding triple-negative breast cancer progression (16). Furthermore, in colon cancer, emodin hinders angiogenesis by inhibiting the expression of acyl-CoA synthetase long-chain family member 4 (17).

Emodin has been shown to inhibit the development of bladder cancer (18,19). Hence, investigating whether emodin can counteract BZ-induced UTUC progression may provide valuable insights into mitigating the adverse health effects of BZ exposure and further understanding the broader impact of emodin on UC.

Materials and methods

Cell culture. BFTC909 cells were purchased from Shanghai Chuanqiu Biotechnology Co., Ltd. and incubated in DMEM/F12 (HyClone; Cytiva) supplemented with 10% fetal bovine serum (FBS; HyClone; Cytiva) at 37˚C with 5% CO_2. UM-UC-14 cells were purchased from Shanghai Fusheng Industrial Co., Ltd. and cultured in Eagle's minimum essential medium (Gibco; Thermo Fisher Scientific, Inc.) supplemented with 2 mM L-glutamine, 10% FBS, antibiotic-antimycotic and 1% non-essential amino acids at 37˚C with 5% CO_2.

Western blotting. The cells were incubated with high-efficiency RIPA lysis buffer (Beijing Solarbio Science & Technology Co., Ltd.) on ice for 5 min. After centrifugation at 11,000 x g for 20 min at 4˚C, the supernatant was collected, and the protein concentration was determined using a BCA kit (Beijing Solarbio Science & Technology Co., Ltd.). Then, 20 μg/lane of sample was separated by 12.5% SDS-PAGE and transferred to a PVDF membrane, followed by incubation with 8% skim milk powder (Thermo Fisher Scientific, Inc.) at room temperature for 2 h. After washing with PBST (0.1% Tween) three times, the PVDF membrane was incubated with the following primary antibodies: Anti-PKA (cat. no. ab75991; 1:1,000), anti-COX2 (cat. no. ab179800; 1:1,000), anti-MMP9 (cat. no. ab76003; 1:1,000), anti-VEGF (cat. no. ab32152; 1:1,000) and anti-GAPDH (cat. no. ab8245; 1:3,000) (all primary antibodies were purchased from Abcam) at 4˚C overnight. After three washes with PBST, the PVDF membranes were incubated with HRP-labeled secondary antibodies [1:5,000; cat. nos. SE131 (anti-mouse) and SE134 (anti-rabbit); Beijing Solarbio Science & Technology Co., Ltd.] at room temperature for 2 h. Subsequently, the protein expression signals were detected with ECL Western Blotting Substrate (Beijing Solarbio Science & Technology Co., Ltd.). GAPDH was used as an internal reference and ImageJ software (version 1.53a; National Institutes of Health; https://imagej.nih.gov/ij/) was used for analysis.

Cell Counting Kit-8 (CCK-8) assay. BFTC909 and UM-UC-14 cells were inoculated into 96-well cell culture plates at 1,000 cells per well and incubated at 37˚C overnight. Subsequently, the cells were divided into the control, BZ (Sigma-Aldrich; Merck KGaA; 1, 5, 10 and 50 nM), and emodin (Sigma-Aldrich; Merck KGaA; 12.5, 25, 50, 100 and 200 μM) groups and incubated at 37˚C for 48 h. Then, 10 μl CCK-8 solution (Beijing Solarbio Science & Technology Co., Ltd.) was added to each well and the cells were incubated at 37˚C for 4 h. Finally, the absorbance was measured at 450 nm, and three replicate wells were set up for each group.

Determination of cAMP concentration and lactate dehydrogenase (LDH) leakage. BFTC909 and UM-UC-14 cells were lysed by sonication in an ice bath and centrifuged at 5,000 x g for 20 min at 4˚C. After the supernatant was collected, the intracellular cAMP and LDH concentrations were analyzed using the cAMP Assay Kit (cat. no. ab65355; Abcam) and LDH Assay Kit (cat. no. ab102526; Abcam) according to the manufacturer's instructions.

Wound healing assay. BFTC909 and UM-UC-14 cells were inoculated at $5x10^5$ cells/well in 6-well plates and incubated overnight. The next day, the cells were gently scraped with a 200 μl pipette tip, then washed well with PBS (this was noted as 0 h). Next, the BFTC909 and UM-UC-14 cells were treated with 10 nM BZ or 50 μM emodin at 37˚C for 24 h in medium containing 2% serum. Representative images at 0 and 24 h were collected using a light microscope (Olympus Corporation), and the wound healing area was recorded (S1 represented the initial wound area, and S2 represented the wound area after 24 h of treatment). The cell migration rate (%) was calculated as [(S1-S2)/S1] x100%, and each set of experiments was repeated three times. ImageJ software (version 1.53a; National Institutes of Health; https://imagej.nih.gov/ij/) was used for analysis.

Transwell assay. In brief, both BFTC909 and UM-UC-14 cells were seeded at a concentration of $1x10^4$ in the upper chamber with 200 μl serum-free DMEM. Then, 600 μl DMEM containing 10% FBS was added to the lower chambers

at 37˚C for 24 h. Subsequently, the cells that migrated to the lower chamber were fixed with 4% paraformaldehyde (Beijing Solarbio Science & Technology Co., Ltd.) at room temperature for 20 min and stained with 0.1% crystal violet for 20 min at room temperature. Representative images were observed under a light microscope (Olympus Corporation). ImageJ software (version 1.53a; National Institutes of Health; https://imagej.nih.gov/ij/) was used for analysis.

Small interfering RNA (siRNA) transfection. BFTC909 and UM-UC-14 cells were inoculated at a density of $5x10^5$ cells/well in 6-well plates and incubated overnight. Next, 10 μl siRNA targeting COX2 (sense, 5'-AAAUUUGAACAAUAAUUUGGU-3'; antisense, 5'-CAAAUUAUUGUUCAAAUUUAG-3') or negative control (NC; sense, 5'-UUCUCCGAACGUGUCACGUTT-3'; antisense, 5'-ACGUGACACGUUCGGAGAATT-3') (Shanghai GenePharma Co., Ltd.) was added to serum-free medium to achieve a final concentration of 20 nM. Then, 10 μl HiPerFect Transfection Reagent (Qiagen GmbH) was added to the siRNA solution. The mixture was incubated at room temperature for 15 min to form siRNA-HiPerFect complexes. The complexes were carefully added to the respective wells and incubated at 37˚C in a 5% CO_2 incubator for 24 h. After the incubation period, the cells were collected for subsequent experiments.

Sp-8-CPT-cAMPS treatment. The cells were divided into four groups for treatment: i) Control (Con) group, cells were treated with 10 nM BZ alone for 48 h; ii) emodin group, cells were pretreated with 50 μM emodin for 1 h, followed by the addition of 10 nM BZ for 48 h; iii) Sp-8-CPT-cAMPS group, cells were pretreated with 10 μM Sp-8-CPT-cAMPS (cat. no. HY-120994B; MedChemExpress) for 1 h, followed by the addition of 10 nM BZ for 48 h; and iv) emodin + Sp-8-CPT-cAMPS group, cells were pretreated with a combination of 10 μM Sp-8-CPT-cAMPS and 50 μM emodin for 1 h, followed by the addition of 10 nM BZ for 48 h. Then, the cells were collected for further assay.

Detection of intracellular malondialdehyde (MDA), superoxide dismutase (SOD), reactive oxygen species (ROS) and total antioxidant capacity. Intracellular MDA, SOD, ROS and total antioxidant capacity were analyzed using a Lipid Peroxidation MDA Assay Kit (cat. no. S0131M; Beyotime Institute of Biotechnology), Reactive Oxygen Species Assay Kit (cat. no. S0033S; Beyotime Institute of Biotechnology), Total Superoxide Dismutase Assay Kit (cat. no. S0101S; Beyotime Institute of Biotechnology) and Total Antioxidant Capacity Assay Kit (cat. no. S0121; Beyotime Institute of Biotechnology), respectively. All operations were carried out in strict accordance with the instruction manuals.

Intracellular Ca^{2+} assay. Detection of intracellular calcium ion levels was accomplished using an Intracellular Ca^{2+} Calcium Ion Assay Kit (cat. no. HR8227; Beijing Biolab Technology Co., Ltd.). Briefly, BFTC909 and UM-UC-14 cells were collected, and F04 staining solution was incubated with the cells at 37˚C for 30 min, after which the intracellular Ca^{2+} content was detected (excitation wavelength of 488-495 nm and emission wavelength of 516 nm).

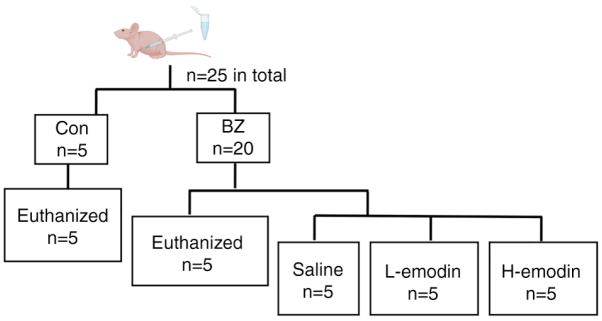

Figure 1. Schematic diagram of the animal experimental design. BZ, benzidine; Con, control.

JC-1 staining. The cells were initially divided into four groups: The control, emodin (50 μM), BZ (10 nM) and BZ + emodin groups. BFTC909 and UM-UC-14 cells were then treated with the indicated drugs for 24 h. Subsequently, the cells were co-incubated with a final concentration of 1 μM JC-1 dye at 37˚C for 30 min. After staining, the cells were washed with PBS and observed under a fluorescence microscope (Olympus Corporation) to assess changes in the mitochondrial membrane potential. At low membrane potentials, JC-1 emits green fluorescence as a monomer, whereas at higher potentials, JC-1 forms 'J-aggregates', emitting red fluorescence.

Nude mouse tumor assay. SPF male BALB/c-nu nude mice (6-8 weeks old; n=25) weighing 15-20 g were obtained from Jinzhou Medical University Experimental Animal Center (Jinzhou, China). All mice were kept in housing with free access to food and water, in an environment with a temperature of 20-24˚C and a humidity level of 45-55% throughout a 12 h light/dark cycle. In the experiment, a BFTC909 cell suspension was prepared at a density of $5x10^7$ cells/ml, 0.1 ml was then subcutaneously inoculated into the dorsal region of the nude mice to construct UTUC transplantation tumors. The tumor formation time was 14 days. Subsequently, the nude mice were divided into two groups: The control (n=5) and BZ (n=20) groups (Fig. 1). In the BZ group, nude mice were administered BZ at a dose of 22 mg/kg body weight in 1 ml of water per dose via gavage for 5 consecutive days, based on previous studies (20,21). The control group was administered an equal volume of water. Subsequently, nude mice in the control and BZ groups (n=5 for each group) were sacrificed, and the tumor volume was evaluated as follows: tumor volume=length x $width^2/2$. After evaluation, the remaining 15 nude mice in the BZ group were randomly divided into three groups: the Control (Con) vehicle group, the Low-dose emodin (L-emodin) group, and the High-dose emodin (H-emodin) group. The Control vehicle group received 1 ml of 2% DMSO in saline by gavage once daily. The L-emodin group was administered emodin at a dose of 40 mg/kg intraperitoneally in 1 ml of PBS once daily, while the H-emodin group received emodin at a dose of 80 mg/kg intraperitoneally in 1 ml of PBS once daily. The entire intervention process lasted for 4 weeks.

The humane endpoints used to determine when animals should be euthanized were severe behavioral abnormalities, such as persistent self-mutilation or inability to move normally. The entire intervention process lasted for 4 weeks, and the

tumor formation time was 14 days. Thus, the total duration of the experiment was 6 weeks. No animals were euthanized before the end of the study. There were also no instances of animal death due to the experimental procedures. Animal health and behavior were monitored once daily. For anesthesia, the mice were anesthetized using isoflurane, with an induction concentration of 2-3% and a maintenance concentration of 1.5-2%. Deep anesthesia was confirmed by the absence of a response to a paw pinch and the absence of a corneal reflex, following ethical guidelines for animal experimentation. Once deep anesthesia was achieved, ~0.6 ml of cardiac blood was collected via cardiac puncture. Death was verified by confirming the absence of a response to a paw pinch and the absence of a corneal reflex. After blood collection, the subcutaneous xenograft tumors were harvested for further experiments, including the determination of cAMP and PGE2 levels, western blotting and immunohistochemistry (IHC).

Detection of alanine aminotransferase (ALT), aspartate aminotransferase (AST), creatinine and urea levels. The blood samples were centrifuged at 1,500 x g for 10 min at 4˚C to separate the serum. An automated biochemical analyzer (Hitachi High-Technologies, Japan) was used to measure the ALT, AST, creatinine and urea levels in the serum, using the respective detection kits: ALT Detection Kit, AST Detection Kit, Creatinine Detection Kit and Urea Detection Kit (all from Zybio Inc.).

IHC. Tumor tissues were fixed using 4% paraformaldehyde (Beijing Solarbio Science & Technology Co., Ltd.) for 24 h at room temperature. After fixation, the tissues were dehydrated with gradient alcohol, cleared with xylene and finally embedded in paraffin. Specifically, the embedded tissues were cut into 5 μm-thick sections, sequentially placed in xylene (three times, 10 min each), gradient alcohol (100, 95, 85 and 70%, 5 min each), and finally washed with distilled water. The tissue sections were autoclave-treated in sodium citrate buffer (pH 6.0; Beijing Solarbio Science & Technology Co., Ltd.) for 15 min. After deparaffinization and rehydration, sections were incubated with 3% hydrogen peroxide (cat. no. H1009; MilliporeSigma) in methanol for 10 min at room temperature to quench endogenous peroxidase activity. Afterwards, the sections were blocked with a solution containing 5% BSA (Thermo Fisher Scientific, Inc.) for 30 min at room temperature. A Ki-67 (1:50; cat. no. 9449, CST Biological Reagents Co., Ltd.) primary antibody was added dropwise to the tissue sections and incubated overnight at 4˚C in a wet box. The sections were subsequently washed three times with PBS for 5 min each. Biotinylated secondary antibodies (1:50; cat. no. SHB131; Beijing Solarbio Science & Technology Co., Ltd.) were added to the sections and incubated for 60 min at room temperature. The sections were washed three times with PBS for 5 min each. DAB color development solution (OriGene Technologies, Inc.) was added dropwise to the sections and incubated for 3 min at room temperature, then the reaction was terminated with distilled water. The nuclei were lightly stained with hematoxylin (Beijing Solarbio Science & Technology Co., Ltd.) for 30 sec at room temperature and washed with tap water. Subsequently, the sections were dehydrated with gradient alcohol, cleared with xylene, and blocked with neutral gum (Beijing Solarbio Science & Technology Co., Ltd.). The sections were finally visualized with a light microscope (BZ-X; Keyence Corporation). ImageJ software (version 1.53a; National Institutes of Health; https://imagej.nih.gov/ij/) was used for analysis. The Ki-67 positive cell rate=(Ki-67 positive cells/total cells) x100%.

Immunofluorescence (IF). The cells were fixed in 4% paraformaldehyde for 15 min at room temperature. The cells were subsequently washed three times with PBS for 5 min each, then permeabilized with 0.3% Triton X-100 (in PBS) for 10 min at room temperature. The cells were blocked with 5% BSA (Thermo Fisher Scientific, Inc.) for 1 h at room temperature, followed by overnight incubation with a COX2 primary antibody (1:50; cat. no. ab179800; Abcam) in a wet box at 4˚C. The cells were subsequently washed three times with PBS for 5 min each. The cells were incubated with goat anti-rabbit IgG/Cy3 (1:200; cat. no. K1034G-Cy3; Beijing Solarbio Science & Technology Co., Ltd.) in a wet box protected from the light for 1 h at room temperature. The cells were incubated with Hoechst (Beijing Solarbio Science & Technology Co., Ltd.) for 10 min at room temperature, then washed three times with PBS for 5 min each time. The coverslips were sealed with a sealer containing an anti-fluorescence attenuation reagent (Beijing Solarbio Science & Technology Co., Ltd.). The cells were observed using a fluorescence microscope (Keyence Corporation).

Statistical analysis. The data are presented as the mean ± standard deviation and were analyzed using Prism 9.0 (Dotmatics). Comparisons between two groups were made using unpaired Student's t-test, and comparisons between more than two groups were made using one-way ANOVA followed by Tukey's HSD test. $P<0.05$ was considered to indicate statistically significant difference.

Results

BZ promotes UTUC tumor growth. The impact of BZ on the viability of BFTC and UM-UC-14 cells was initially investigated. As shown in Fig. 2A and B, BZ significantly enhanced the viability of both cell lines at concentrations of 1, 5, 10 and 50 nM. Furthermore, the wound healing and Transwell assays demonstrated that BZ facilitated the migration of BFTC and UM-UC-14 cells (Fig. 2C-F). Subsequent *in vivo* experiments further validated these findings, indicating that BZ promoted subcutaneous tumor growth in nude mice (Fig. 2G). IHC staining revealed that BZ increased the percentage of Ki-67-positive cells compared with the control group (Fig. 2H).

Emodin decreases cell viability and mitochondrial membrane potential in BZ-Induced malignant cells. It was next evaluated whether emodin could inhibit BZ-induced malignant cell survival *in vitro*. Compared with BZ alone (10 nM), emodin significantly reduced the viability of both BFTC and UM-UC-14 cells (at concentrations of 12.5, 25, 50, 100, and 200 μM) in a concentration-dependent manner (Fig. 3A and B). The LDH leakage rate, a critical indicator of cell damage, was significantly lower in the BZ-treated group than in the control

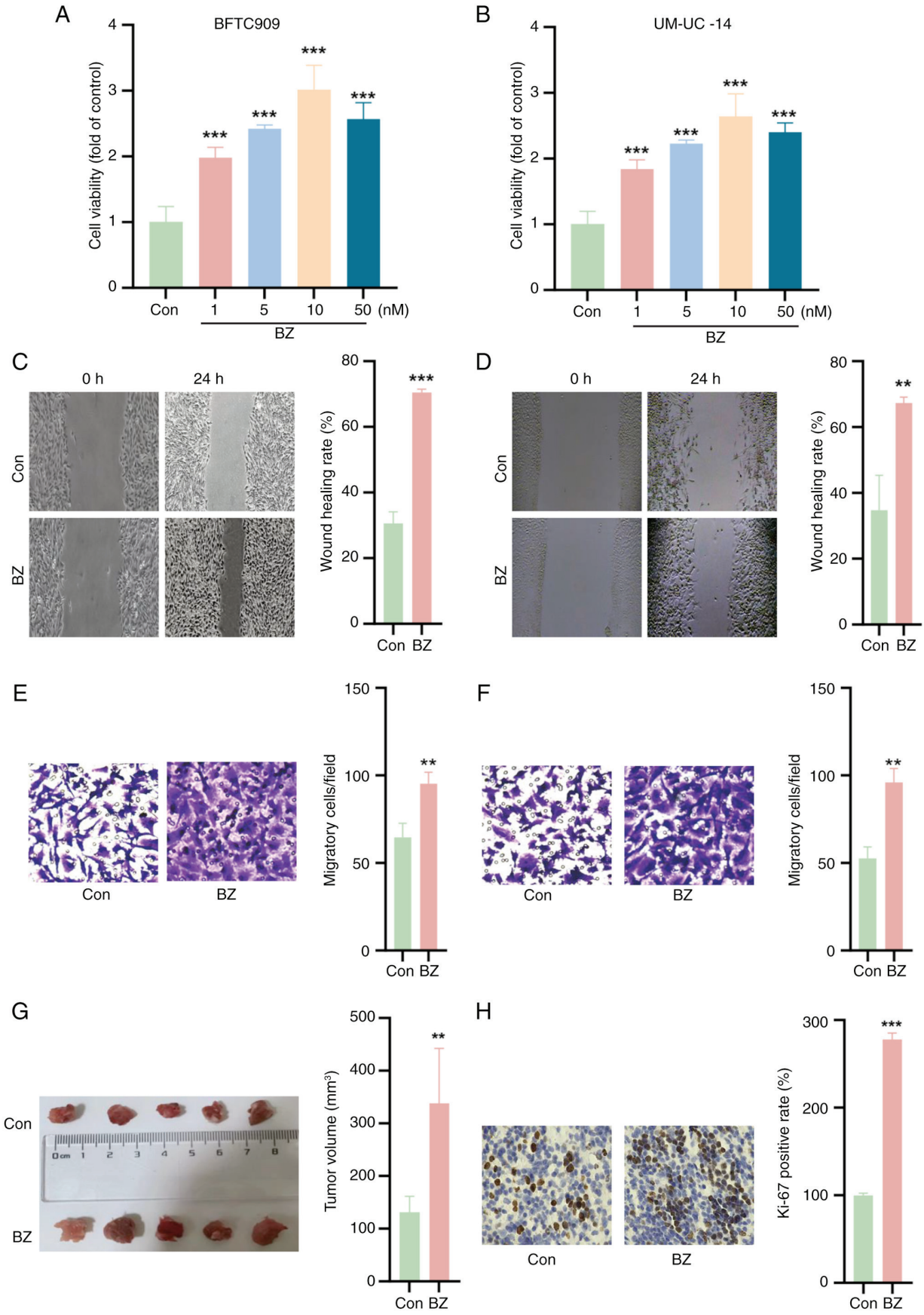

Figure 2. BZ promotes upper urinary tract urothelial carcinoma cell growth. Cell Counting Kit-8 assays were used to explore the effects of BZ (1, 5, 10 and 50 nM for 24 h) on the viability of (A) BFTC and (B) UM-UC-14 cells. Wound healing assays demonstrating the migratory capacity of (C) BFTC and (D) UM-UC-14 cells upon BZ treatment (10 nM BZ at 37˚C for 48 h); magnification, x4. Transwell assays demonstrating the migratory capacity of (E) BFTC and (F) UM-UC-14 cells upon BZ treatment (10 nM BZ at 37˚C for 48 h); magnification, x20. (G) *In vivo* experiments confirming the promotion of subcutaneous tumor growth in nude mice following BZ administration (22 mg/kg body weight for 5 consecutive days). (H) Immunohistochemistry staining showing that, compared with Con, BZ increased the percentage of Ki-67-positive cells; magnification, x20. **P<0.01, ***P<0.001 vs. Con. BZ, benzidine; Con, control.

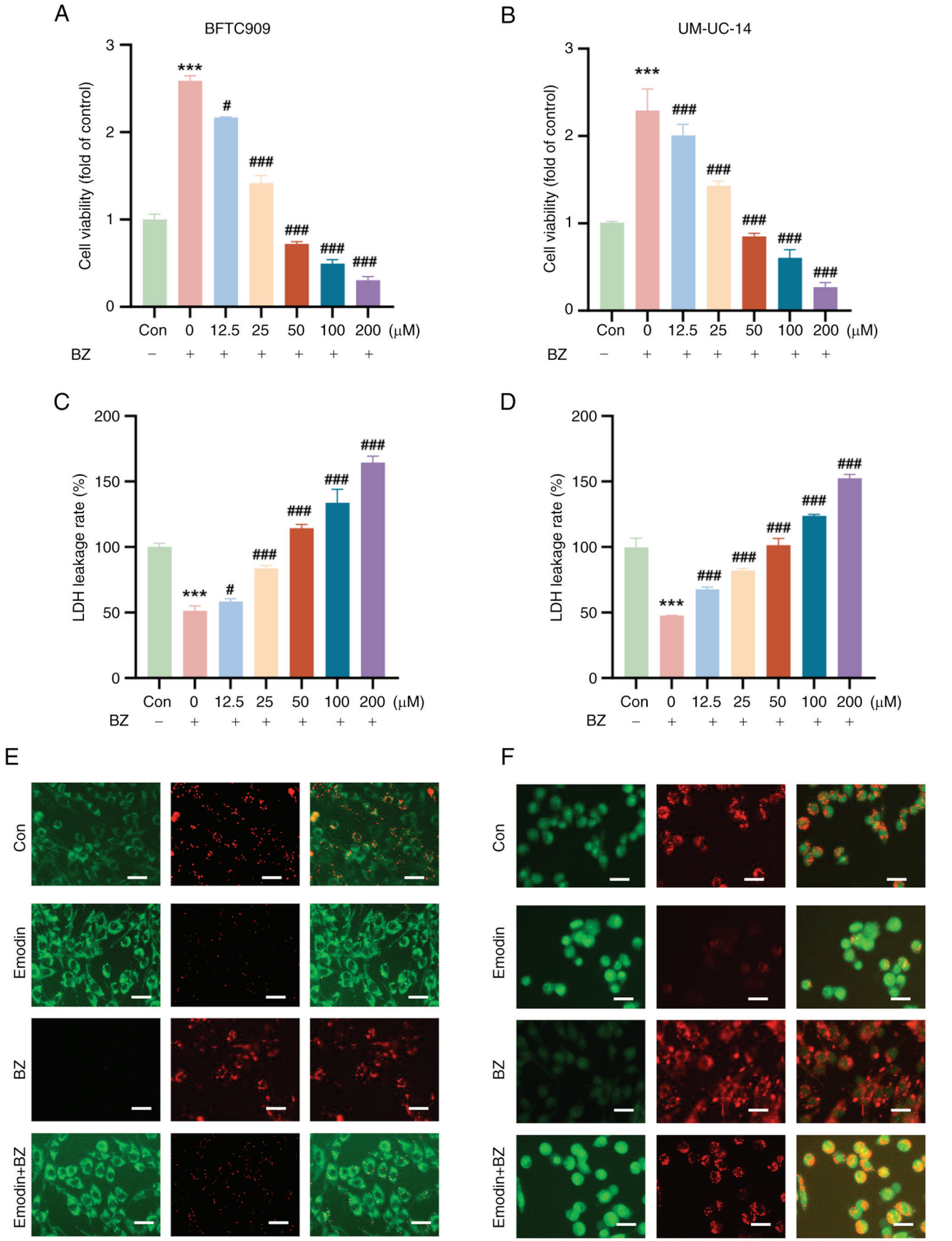

Figure 3. Emodin suppresses BZ-increased viability and induces cellular damage in bladder cancer cells. BFTC and UM-UC-14 cells were preincubated with varying concentrations of emodin (12.5, 25, 50, 100 and 200 μM) at 37˚C for 1 h. Then, the cells were further treated with 10 nM BZ at 37˚C for another 48 h in the presence of emodin at the indicated concentrations. The dose-dependent inhibitory effects of emodin on the viability of (A) BFTC and (B) UM-UC-14 cell lines treated with varying concentrations of emodin (12.5, 25, 50, 100 and 200 μM) compared with cells treated with BZ alone. Effect of emodin treatment on LDH leakage in (C) BFTC and (D) UM-UC-14 cell lines. JC-1 staining showed changes in the mitochondrial membrane potential in (E) BFTC and (F) UM-UC-14 cells. ***P<0.001 vs. Con; $^{\#}$P<0.05, $^{\#\#\#}$P<0.001 vs. BZ alone. BZ, benzidine; Con, control; LDH, lactate dehydrogenase.

group; however, emodin treatment increased the LDH leakage rate (Fig. 3C and D). Changes in mitochondrial membrane potential were assessed using the JC-1 staining method. JC-1 is a commonly used fluorescent probe for evaluating mitochondrial membrane potential; it forms aggregates and emits red fluorescence at high membrane potential, while at low membrane potential, it remains in the monomeric form and emits green fluorescence. In this experiment, strong red fluorescence was observed in the untreated control group, indicating a high mitochondrial membrane potential. Compared with the control, cells treated with emodin showed a significant decrease in red fluorescence and an increase in green fluorescence in both BFTC and UM-UC-14 cells, indicating a decrease in mitochondrial membrane potential. Even in the presence of BZ, emodin effectively lowered the mitochondrial membrane potential, as evidenced by the reduced red and increased green fluorescence (Fig. 3E and F).

BZ activates COX2/PKA signaling in UTUC. The effect of BZ on the COX2/PKA signaling pathway was further investigated. It was observed that BZ significantly upregulated the protein expression of PKA and COX2 in BFTC and UM-UC-14 cells transfected with si-NC (Fig. 4A and B). To investigate the role of COX2 in BZ-induced PKA signaling activation, siRNAs specifically targeting COX2 were screened. si-COX2 effectively downregulated COX2 expression and subsequently reduced PKA expression. Furthermore, COX2 knockdown reversed the BZ-induced increase in PKA expression. These findings indicated that BZ-mediated activation of PKA signaling was achieved through the induction of COX2 (Fig. 4A and 4B). Additionally, BZ treatment led to increased levels of cAMP and PGE2 in cell lysates, but si-COX2 reversed these effects with or without BZ treatment (Fig. 4C-F). *In vivo*, BZ also elevated the protein expression of PKA and COX2 in tumor tissues from nude mice (Fig. 4G) and increased the levels of cAMP and PGE2 within these tumors (Fig. 4H and I).

Emodin inhibits cAMP/PKA/COX2 signaling in UTUC cells in the presence of BZ. It was also investigated whether emodin inhibits the cAMP/PKA/COX2 signaling pathway in UTUC cells in the presence of BZ. The findings indicated that emodin combined with BZ markedly decreased cAMP levels in BFTC909 and UM-UC-14 cells compared with BZ treatment alone (Fig. 5A and B). Additionally, western blotting analysis revealed that emodin significantly suppressed the expression of PKA and the downstream effector COX2 in these cells at concentrations of 25 and 50 μM, compared with BZ treatment alone (Fig. 5C and D). Additionally, IF experiments confirmed that BZ increased COX2 expression in BFTC909 and UM-UC-14 cells, while emodin treatment reduced the BZ-induced increase in COX2 expression (Fig. 5E).

Emodin inhibits the survival of UTUC cells by inhibiting PKA signaling when combined with BZ. To further investigate the capacity of emodin to suppress the malignant phenotype of UTUC cells by inhibiting PKA signaling, the BFTC909 and UM-UC-14 cells were preincubated with BZ before further treatment. Subsequent exposure to Sp-8-CPT-cAMPS, a PKA activator, resulted in a significant increase in PKA and COX2 protein levels, as demonstrated by western blotting analysis (Fig. 6A and B). Notably, the emodin-induced downregulation of PKA and COX2 expression was partially reversed by Sp-8-CPT-cAMPS. Additionally, while emodin significantly reduced the PGE2 levels, treatment with Sp-8-CPT-cAMPS led to an increase in PGE2 production and it significantly reversed the reduction caused by emodin (Fig. 6C and D). In terms of cell viability, compared with the control, Sp-8-CPT-cAMPS notably enhanced the survival of BFTC909 and UM-UC-14 cells, and it notably mitigated the emodin-induced decrease in cell viability (Fig. 6E and F). These findings suggest that emodin effectively inhibits the viability of UTUC cells predominantly through the inhibition of PKA signaling.

Emodin reduces UTUC cell migration by inhibiting MMP9 and VEGF. Previous studies have shown that PGE2 enhances tumor cell infiltration and metastasis by upregulating MMP9 and VEGF (22,23). In the present study, the effects of emodin on the expression of these critical proteins was investigated. The BFTC909 and UM-UC-14 cells were preincubated with 10 nM BZ before further treatment. It was observed that emodin significantly reduced the expression of MMP9 and VEGF in both BZ-treated BFTC909 and UM-UC-14 cells compared with the control cells. Conversely, treatment with Sp-8-CPT-cAMPS alone led to an increase in the expression of these proteins (Fig. 7A and B). Notably, Sp-8-CPT-cAMPS also counteracted the suppressive effect of emodin on MMP9 and VEGF expression (Fig. 7A and B). Furthermore, emodin decreased the migration of BFTC909 and UM-UC-14 cells relative to that of control cells, while Sp-8-CPT-cAMPS promoted cell migration (Fig. 7C and D). Most notably, Sp-8-CPT-cAMPS reversed the emodin-induced decrease in migration in these BZ-treated cell lines (Fig. 7C and D).

Emodin inhibits tumor growth in nude mice in vivo. *In vivo* experiments involving nude mice pretreated with BZ confirmed that emodin could effectively decrease the weight and volume of tumors (Fig. 8A-C). Additionally, emodin reduced the levels of cAMP and PGE2 in tumor tissues (Fig. 8D and E). The *in vivo* safety of emodin was also evaluated. The experimental results showed that emodin did not have any significant toxic effects on the liver or kidneys of the treated mice. Liver function tests, including the measurement of ALT and AST enzymes, revealed no significant differences between the emodin-treated group and the control group (Fig. 8F and G). Similarly, kidney function markers, such as creatinine and UREA, remained within the normal ranges, indicating no renal toxicity (Fig. 8H and I). By contrast, emodin decreased the LDH leakage rate in tumor tissues compared with the control tissues (Fig. 8J). Ki-67 staining also showed that L-emodin and H-emodin decreased the percentage of Ki-67-positive cells (Fig. 8K). Furthermore, there was a notable decrease in the expression of MMP9 and VEGF in the tumor tissues of these nude mice (Fig. 8L). These findings collectively indicate that emodin exerts a notable inhibitory effect on tumor development *in vivo*.

Discussion

Bladder cancer ranks as the most prevalent and lethal among common malignant tumors of the urinary system. The primary environmental contributors to bladder cancer

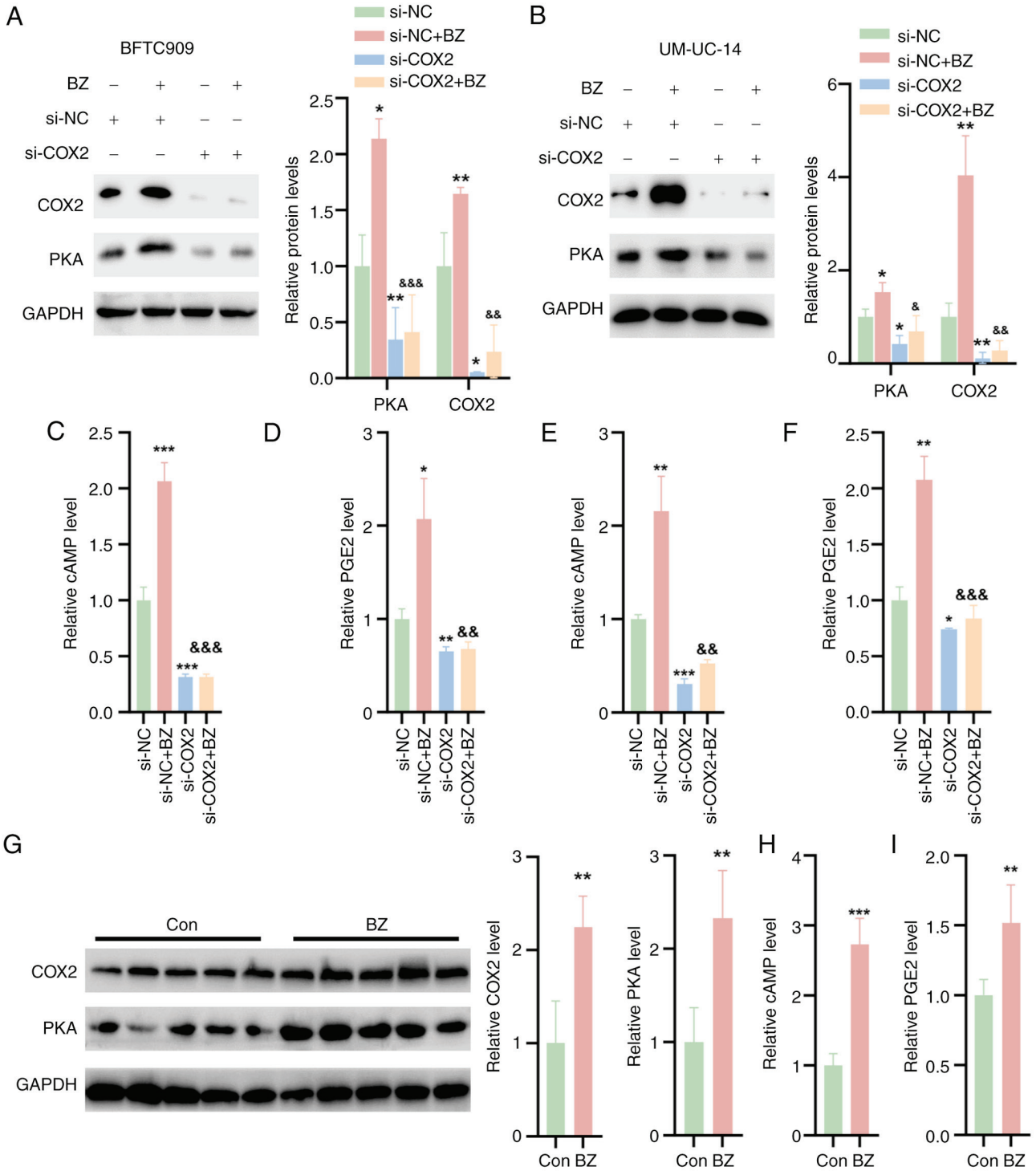

Figure 4. BZ activates COX2/PKA signaling in upper urinary tract urothelial carcinoma cells and tumor tissues. The BFTC and UM-UC-14 cells were divided into four groups as follows: Control group, cells directly transfected with NC siRNA; BZ group, cells treated with 10 nM BZ for 48 h; si-COX2 group, cells transfected with si-COX2 for 48 h; and si-COX2 + BZ group, cells first transfected with si-COX2 for 1 h, followed by coincubation with 10 nM BZ at 37˚C for 48 h. Western blotting analysis indicating the protein expression of PKA and COX2 in (A) BFTC and (B) UM-UC-14 cells treated as aforementioned. The (C) cAMP and (D) PGE2 levels in cell lysates of BFTC cells. The (E) cAMP and (F) PGE2 levels in cell lysates of UM-UC-14 cells. (G) Western blotting analysis indicating the protein levels of PKA and COX2 in tumor tissues from nude mice treated with BZ. The (H) cAMP and (I) PGE2 levels in the tumor tissues of BZ-treated nude mice. *P<0.05, **P<0.01, ***P<0.001 vs. si-NC; $^{\&}$P<0.05, $^{\&\&}$P<0.01, $^{\&\&\&}$P<0.001 vs. si-NC + BZ. BZ, benzidine; cAMP, cyclic adenosine monophosphate; Con, control; COX2, cyclooxygenase 2; PGE2, prostaglandin E2; PKA, protein kinase A; NC, negative control; si, small interfering RNA.

include tobacco smoke, arsenic in drinking water and occupational exposure to aromatic amines (24,25). BZ, known for its carcinogenic properties, has been banned in industrial production (26). Nevertheless, it is still detected in certain food colors. Moreover, with the increase in tobacco use, BZ continues to significantly contribute to the incidence of bladder tumors (26). UTUC, involving tumors of the renal pelvis and ureters, demands careful clinical attention due to its recurring and highly malignant nature (27). Early detection and appropriate treatment can lead to clinical remission (27).

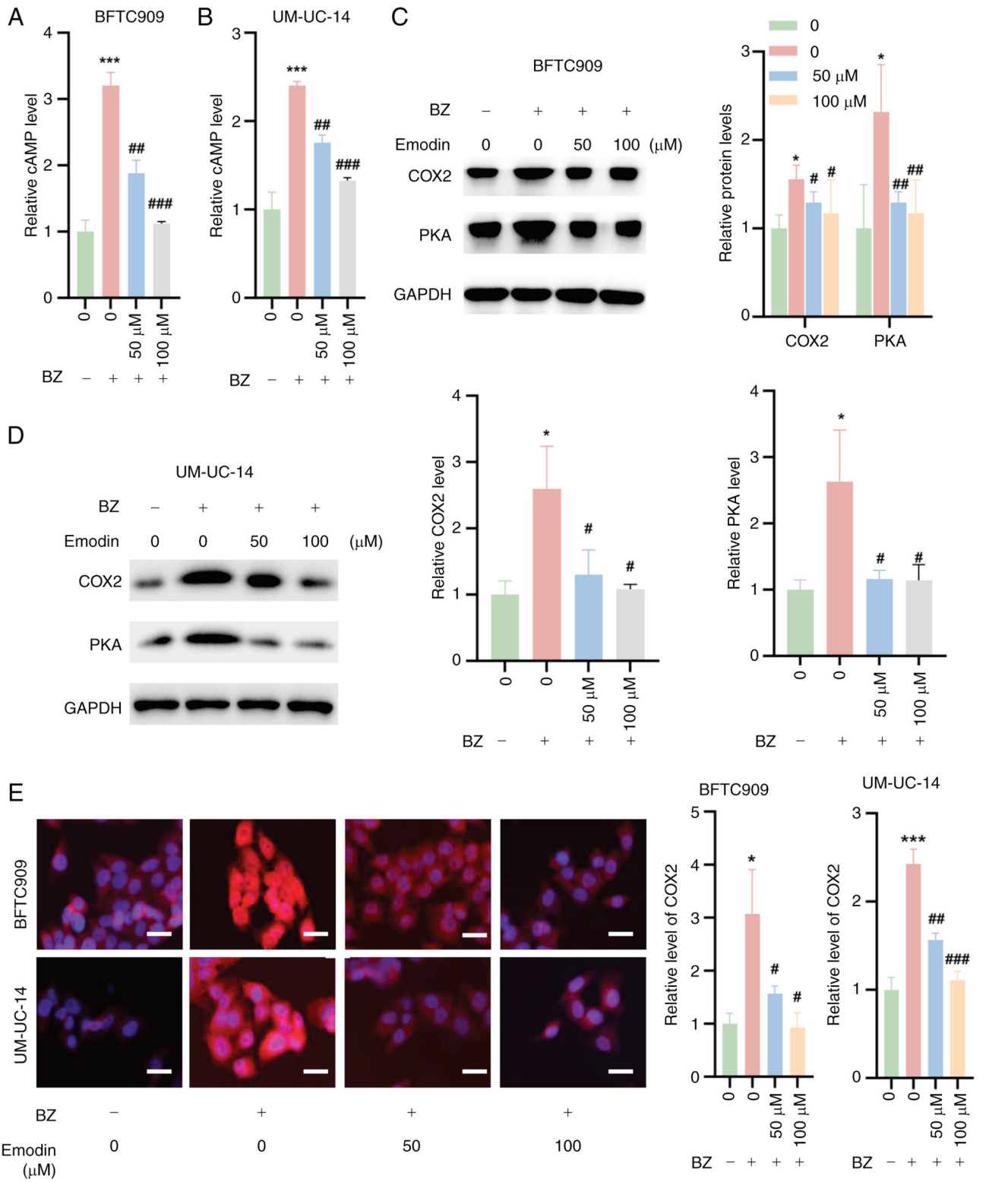

Figure 5. Inhibition of cAMP/PKA/COX2 signaling by emodin in upper urinary tract urothelial carcinoma cells. BFTC and UM-UC-14 cells were preincubated with 50 or 100 μM emodin at 37˚C for 1 h. Then, the cells were further treated with 10 nM BZ at 37˚C for another 48 h in the presence of emodin at the indicated concentrations. cAMP levels in (A) BFTC909 and (B) UM-UC-14 cells treated as aforementioned. Western blotting analysis demonstrating the expression levels of PKA and the downstream signaling molecule, COX2, in (C) BFTC909 and (D) UM-UC-14 cells treated as aforementioned. (E) Immunofluorescence staining indicating COX2 expression in BFTC909 and UM-UC-14 cells treated as aforementioned. *P<0.05, ***P<0.001 vs. 0 μM emodin; $^{\#}$P<0.05, $^{\#\#}$P<0.01, $^{\#\#\#}$P<0.001 vs. BZ + 0 μM emodin. BZ, benzidine; cAMP, cyclic adenosine monophosphate; Con, control; COX2, cyclooxygenase 2; PKA, protein kinase A.

A number of patients with UTUC, particularly older adults, are asymptomatic and are often diagnosed during routine health examinations (28). Notably, the incidence of UTUC is markedly greater among smokers than non-smokers and poses a greater risk to individuals working in petrochemical, plastics and other chemical industries (28). Research on the

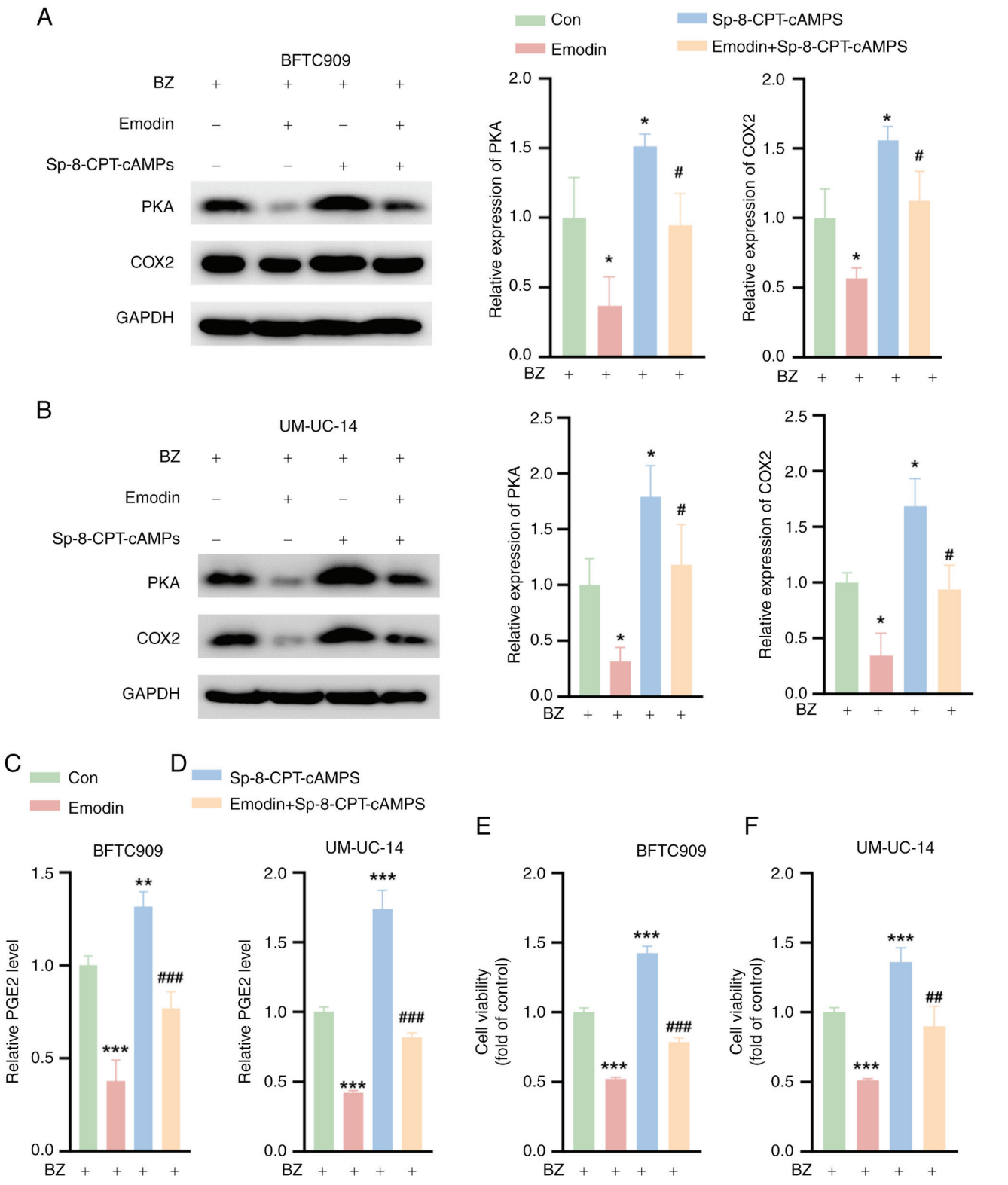

Figure 6. Emodin inhibits the survival of upper urinary tract urothelial carcinoma Cells by inhibiting PKA signaling. The cells were divided into four groups. Con group, cells were treated with 10 nM BZ alone for 48 h; Emodin group, cells were pretreated with 50 μM emodin for 1 h, followed by the addition of 10 nM BZ for 48 h; Sp-8-CPT-cAMPS group, cells were pretreated with 10 μM Sp-8-CPT-cAMPS for 1 h, followed by the addition of 10 nM BZ for 48 h; and Emodin + Sp-8-CPT-cAMPS group, cells were pretreated with a combination of 10 μM Sp-8-CPT-cAMPS and 50 μM emodin for 1 h, followed by the addition of 10 nM BZ for 48 h. Western blotting analysis showing the PKA and COX2 expression levels in (A) BFTC909 and (B) UM-UC-14 cells treated as aforementioned. The PGE2 levels in (C) BFTC909 and (D) UM-UC-14 cells treated as aforementioned. Cell Counting Kit-8 assays indicating the viability of (E) BFTC909 and (F) UM-UC-14 cells treated as aforementioned. *P<0.05, **P<0.01, ***P<0.001 vs. Con; $^{\#}$P<0.05, $^{\#\#}$P<0.01, $^{\#\#\#}$P<0.001 vs. emodin. BZ, benzidine; Con, control; COX2, cyclooxygenase 2; PGE2, prostaglandin E2; PKA, protein kinase A.

mechanisms of BZ-induced UTUC is still limited. To the best of our knowledge, the present study is the first to provide *in vitro* evidence that BZ promotes the survival and migration of UTUC cells, thus supporting tumor growth. These

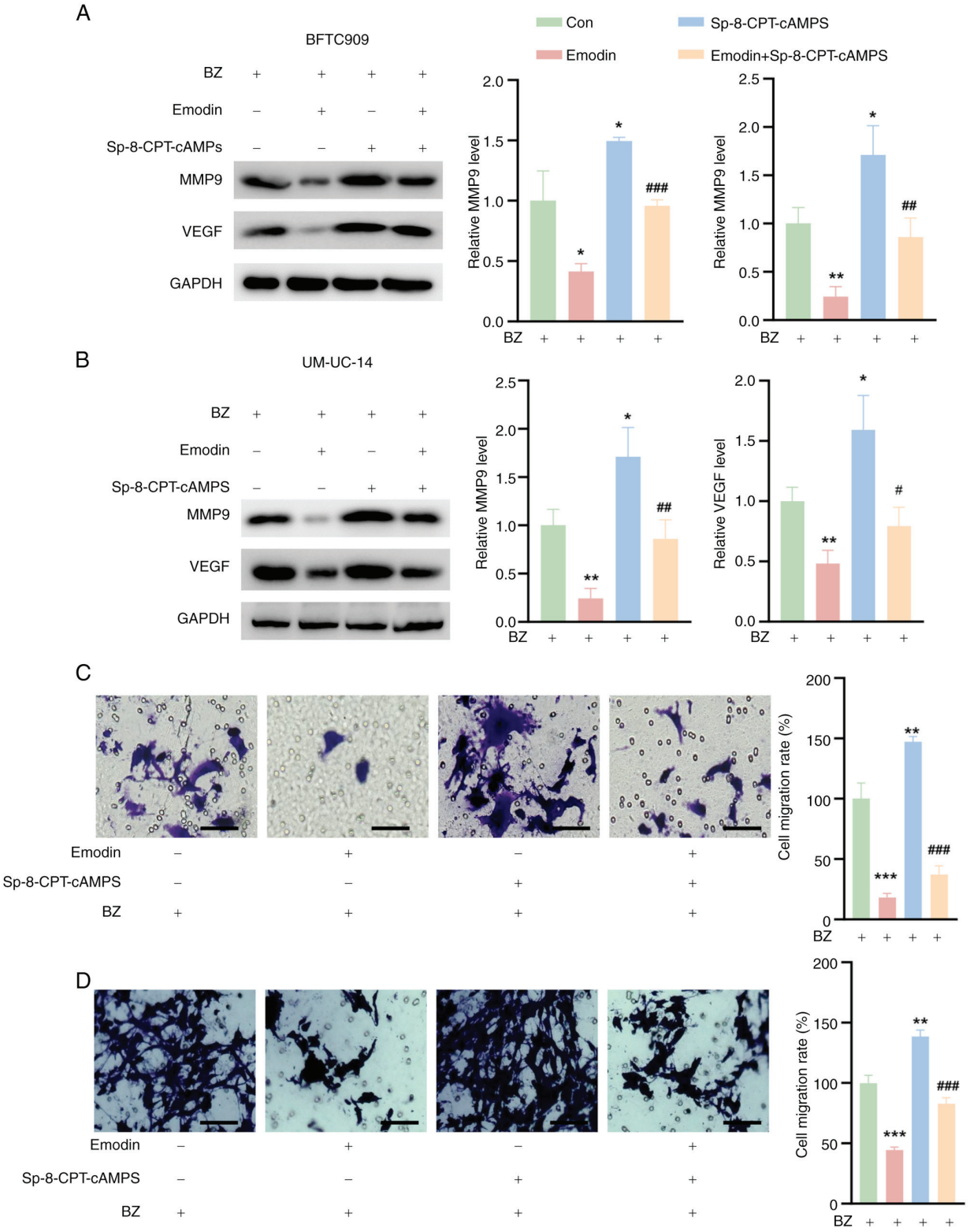

Figure 7. Effects of emodin and Sp-8-CPT-cAMPS on MMP9 and VEGF expression and cell migration in BFTC909 and UM-UC-14 cells. The cells were divided into four groups. Con group, cells were treated with 10 nM BZ alone for 48 h; Emodin group, cells were pretreated with 50 μM emodin for 1 h, followed by the addition of 10 nM BZ for 48 h; Sp-8-CPT-cAMPS group, cells were pretreated with 10 μM Sp-8-CPT-cAMPS for 1 h, followed by the addition of 10 nM BZ for 48 h; and Emodin + Sp-8-CPT-cAMPS group, cells were pretreated with a combination of 10 μM Sp-8-CPT-cAMPS and 50 μM emodin for 1 h, followed by the addition of 10 nM BZ for 48 h. MMP9 and VEGF levels in (A) BFTC909 and (B) UM-UC-14 cells treated as aforementioned. Transwell assay results of (C) BFTC909 and (D) UM-UC-14 cells treated as aforementioned. *P<0.05, **P<0.01, ***P<0.001 vs. Con; $^{\#}$P<0.05, $^{\#\#}$P<0.01, $^{\#\#\#}$P<0.001 vs. emodin. BZ, benzidine; Con, control; MMP9, matrix metalloproteinase 9; VEGF, vascular endothelial growth factor.

findings establish the significant carcinogenic role of BZ in the progression of UTUC.

Natural drugs are increasingly recognized as vital sources for developing therapeutic agents due to their broad

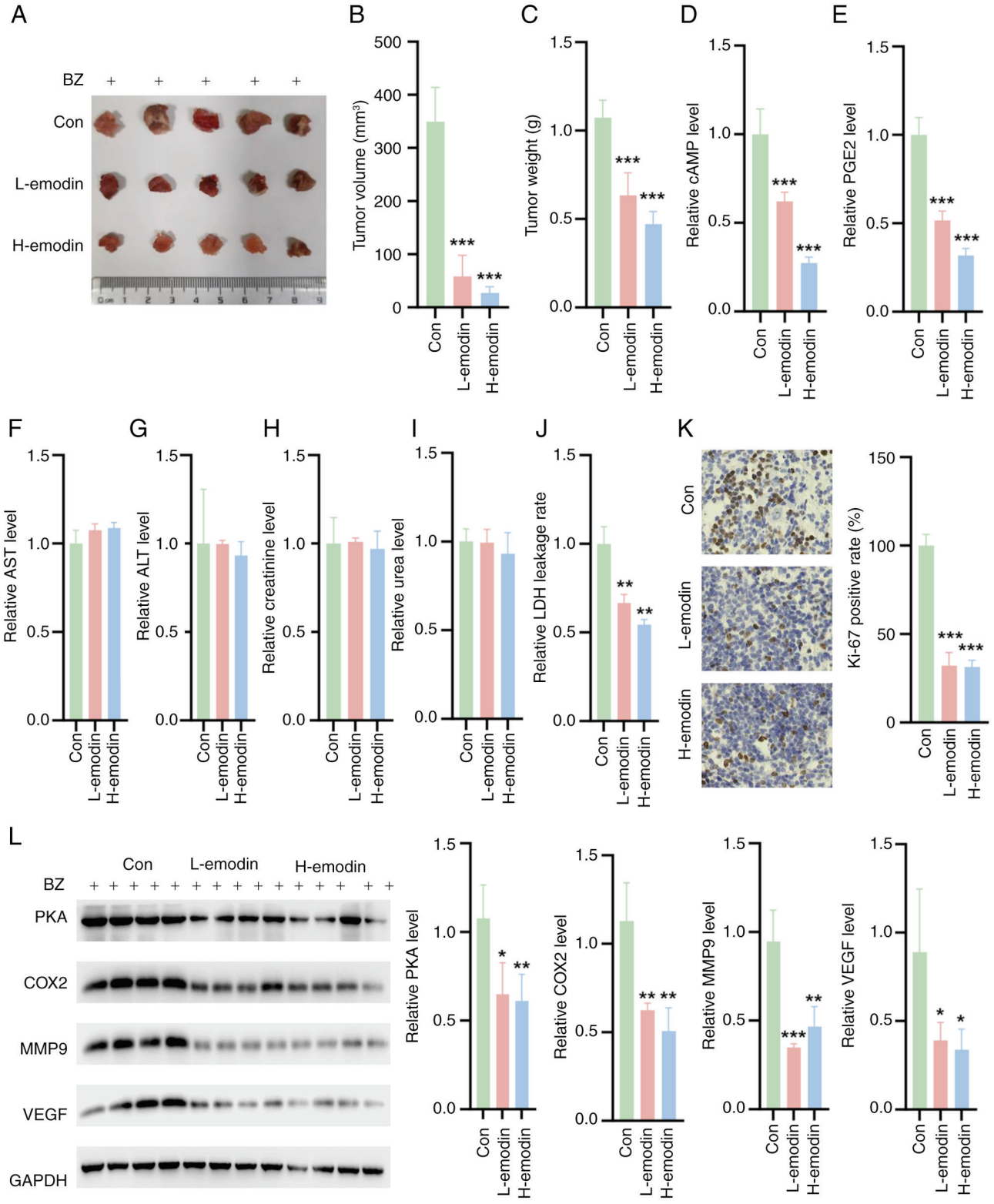

Figure 8. Impact of emodin on tumor growth and biochemical markers in BZ-pretreated nude mice. (A) Representative tumor images. Quantification of the (B) tumor volume and (C) weight. (D) cAMP (D) and (E) PGE2 levels in tumor tissues. Liver function parameters, including (F) ALT and (G) AST levels in the treated mice. Kidney function markers, such as (H) creatinine and (I) 0urea in the treated mice. (J) LDH leakage rate in the tumor tissues. (K) Ki-67 staining of the tumor tissues. (L) The expression levels of PKA, COX2, MMP9 and VEGF in the tumor tissues. *P<0.05, **P<0.01, ***P<0.001 vs. Con. ALT, alanine transaminase; AST, aspartate transaminase; BZ, benzidine; cAMP, cyclic adenosine monophosphate; Con, control; COX2, cyclooxygenase 2; H-emodin, 80 mg/kg emodin; L-emodin, 40 mg/kg emodin; MMP9, matrix metalloproteinase 9; PGE2, prostaglandin E2; PKA, protein kinase A; VEGF, vascular endothelial growth factor.

biological impacts and minimal side effects (16). Among these, *Rheum officinale*, particularly its anthraquinone derivatives extracted from its roots and rhizomes, has shown promising potential due to its anti-inflammatory,

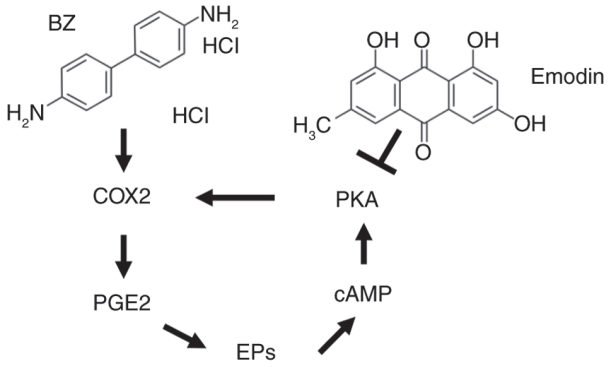

Figure 9. Schematic diagram of the effects of BZ and emodin on the COX2 signaling pathway. BZ, benzidine; cAMP, cyclic adenosine monophosphate; COX2, cyclooxygenase 2; EPs, prostaglandin E receptors; PGE2, prostaglandin E2; PKA, protein kinase A.

antifibrotic, antioxidant, antitumor and antidiabetic properties (29). Despite these known effects, the protective role of emodin, a compound derived from *R. officinale*, against BZ-induced UTUC remains unexplored. The results of the *in vitro* experiments in the present study revealed that emodin can significantly mitigate the BZ-induced increase in UTUC cell viability and decrease the LDH leakage rate. Additionally, emodin attenuated the increase in the mitochondrial membrane potential induced by BZ. These findings preliminarily indicate that emodin may have a crucial protective role in the progression of BZ-induced UTUC, highlighting its potential as a therapeutic agent in oncological treatments.

PGE2, the most prevalent arachidonoid lipid and a lipid metabolite with immunomodulatory functions, has been implicated in the development of various malignant tumors, such as pancreatic cancer, bladder cancer and UTUC (13,30,31). Previous studies have demonstrated that emodin inhibits PGE2 production (32,33). Therefore, the present investigation aimed to evaluate whether BZ activates PGE2-associated signaling pathways to facilitate the viability of UTUC cells. Both the *in vitro* and *in vivo* experiments confirmed that BZ upregulated the expression of PKA and COX2, concomitantly increasing the cAMP and PGE2 levels. The present investigation further revealed that BZ significantly upregulated the expression of VEGF and MMP9, which are pivotal factors implicated in tumor angiogenesis and invasion. These findings not only elucidated the role of BZ in promoting the progression of UTUC but also shed light on its potential carcinogenic effects on the upper urinary tract system, extending beyond its association with bladder cancer. In the EP2-cAMP-PKA signaling pathway, there is a positive feedback loop that regulates the expression of PGE2 and COX2 (34-36). Specifically, activation of PKA leads to an increase in COX2 expression (37-40). This occurs since PKA can phosphorylate and activate transcription factors that upregulate the expression of COX2. Consequently, when a PKA activator is introduced, it enhances PKA activity, which in turn elevates COX2 levels (38-40). Similarly, PGE2 and cAMP are involved in a positive feedback mechanism. PGE2 can increase cAMP levels by binding to its receptor, EP2, which activates adenylate cyclase. This enzyme catalyzes the conversion of ATP to cAMP (38-40). Elevated cAMP levels then activate PKA, which further increases COX2 expression and subsequently PGE2 production. Hence, in the present study, BFTC909 and UM-UC-14 cells, which were pretreated with BZ, were treated with a PKA activator, Sp-8-CPT-cAMPS, to test whether emodin exerts an anti-UTUC effect by targeting the PKA/COX2 signaling pathway. Compared with the control group, emodin treatment resulted in a notable reduction in the expression levels of PKA, COX2, VEGF and MMP9. Furthermore, the emodin-induced decreases in PKA, COX2, VEGF and MMP9 expression were significantly reversed upon the addition of Sp-8-CPT-cAMPS. Based on these extensive research findings, we consider that the current data sufficiently demonstrate the feedback regulation of COX2 by PKA. However, we recognize the importance of directly demonstrating the role of PKA. To address this, we plan to conduct further experiments to directly downregulate PKA using siRNA or pharmacological inhibitors to assess its impact on COX2 expression and the overall signaling pathway.

Moreover, in the present study, in the *in vivo* experiments using nude mice with BZ-induced subcutaneous tumors, emodin administration led to a reduction in tumor volume. Additionally, emodin treatment decreased PGE2 and cAMP levels and reduced MMP9 and VEGF expression. These novel findings highlight the crucial role of emodin in abolishing BZ-associated UTUC development by targeting the PKA/COX2 signaling pathway, indicating that emodin is a promising therapeutic strategy for occupational UTUC treatment. Additionally, the experimental results showed that emodin did not have any significant toxic effects on the liver or kidneys of the treated mice. Liver function tests, including measurements of ALT and AST levels, revealed no significant differences between the emodin-treated group and the control group. Similarly, kidney function markers, such as creatinine and UREA, remained within normal ranges, indicating no renal toxicity. These findings were consistent with previous studies that demonstrated the safety profile of emodin in similar settings (16,19). The lack of hepatotoxicity and nephrotoxicity is particularly notable given the prolonged treatment duration and the relatively high doses used in the experiments of the present study. This finding confirmed that the observed therapeutic effects of emodin on inhibiting BZ-induced cell survival and migration are not confounded by potential organ toxicity. Future studies should continue to monitor these safety parameters in different models and at different doses to further confirm the non-toxic nature of emodin, thereby supporting its potential clinical application in treating UTUC.

In conclusion, emodin inhibits the activity of the PKA/COX2 signaling pathway, thereby suppressing the development of UTUC induced by BZ exposure (Fig. 9). These findings lay the groundwork for a comprehensive understanding of the molecular mechanisms underlying BZ-induced UTUC, highlighting the potential of PKA/COX2 pathway inhibitors as crucial targets for early intervention in UTUC. Hence, emodin has emerged as a promising candidate for both early intervention and therapeutic strategies in UTUC management.

Acknowledgements

Not applicable.

Funding

This study was supported by the Scientific Research Funding Project of Liaoning Provincial Department of Education (grant no. JYTJCZR2020063).

Availability of data and materials

The data generated in the present study may be requested from the corresponding author.

Authors' contributions

YJ performed the experiments and analyzed the data. CW, KF, XW and MT performed the animal experiments. YJ and GT designed all the experiments, analyzed the data and gave final approval for the version to be published. YJ and GT confirm the authenticity of all the raw data. All the authors have read and approved the final version of the manuscript.

Ethics approval and consent to participate

This study involving animals was reviewed and approved by Jinzhou Medical University (*Jinzhou, China;* approval no. 2020-AJ-05).

Patient consent for publication

Not applicable.

Competing interests

The authors declare that they have no competing interests.

References

1. Habil MR and Hein DW: Effects of dose and human N-acetyltransferase 1 genetic polymorphism in benzidine metabolism and genotoxicity. Arch Toxicol 97: 1765-1772, 2023.
2. Dietrich HG and Golka K: Bladder tumors and aromatic amines-historical milestones from Ludwig Rehn to Wilhelm Hueper. Front Biosci (Elite Ed) 4: 279-288, 2012.
3. Durgaryan R and Durgaryan N: Chemical oxidative condensation of benzidine in non-aqueous medium: Synthesis and investigation of oligomers and polymer with Benzidine Diimine Units. Polymers (Basel) 14: 34, 2021.
4. Suarez-Torres JD, Orozco CA and Ciangherotti CE: Applying Bayesian forecasting to predictive toxicology: The probability of innate carcinogenicity to humans of colorants synthesized from benzidine. Toxicol Lett 351: 111-134, 2021.
5. Kenigsberg AP, Meng X, Ghandour R and Margulis V: Oncologic outcomes of radical nephroureterectomy (RNU). Transl Androl Urol 9: 1841-1852, 2020.
6. Bayerl F, Meiser P, Donakonda S, Hirschberger A, Lacher SB, Pedde AM, Hermann CD, Elewaut A, Knolle M, Ramsauer L, *et al*: Tumor-derived prostaglandin E2 programs cDC1 dysfunction to impair intratumoral orchestration of anticancer T-cell responses. Immunity 56: 1341-1358 e11, 2023.
7. Woolbright BL, Pilbeam CC, Taylor JA III: Prostaglandin E2 as a therapeutic target in bladder cancer: From basic science to clinical trials. Prostaglandins Other Lipid Mediat 148: 106409, 2020.
8. Kissoondoyal A and Crawford DA: Prostaglandin E2 increases neurite length and the formation of axonal loops, and regulates cone turning in differentiating NE4C Cells Via PKA. Cell Mol Neurobiol 42: 1385-1397, 2022.
9. Chang HH, Young SH, Sinnett-Smith J, Chou CE, Moro A, Hertzer KM, Hines OJ, Rozengurt E and Eibl G: Prostaglandin E2 activates the mTORC1 pathway through an EP4/cAMP/PKA- and EP1/Ca2+-mediated mechanism in the human pancreatic carcinoma cell line PANC-1. Am J Physiol Cell Physiol 309: C639-C649, 2015.
10. Zhao P, Li XG, Yang M, Shao Q, Wang D, Liu S, Song H, Song B, Zhang Y and Qu X: Hypoxia suppresses the production of MMP-9 by human monocyte-derived dendritic cells and requires activation of adenosine receptor A2b via cAMP/PKA signaling pathway. Mol Immunol 45: 2187-2195, 2008.
11. Fang XL, Zhang Q, Xue WW, Tao JH, Zou HD, Lin QR and Wang YL: Suppression of cAMP/PKA/CREB signaling ameliorates retinal injury in diabetic retinopathy. Kaohsiung J Med Sci 39: 916-926, 2023.
12. Jeon HG, Jeong IG, Bae J, Lee JW, Won JK, Paik JH, Kim HH, Lee SE and Lee E: Expression of Ki-67 and COX-2 in patients with upper urinary tract urothelial carcinoma. Urology 76: 513 e7-12, 2010.
13. Komatsu M, Funakoshi T, Aki T, Unuma K and Uemura K: Aristolochic acid induces an inflammatory response with prostaglandin E2 production and apoptosis in NRK-52E proximal tubular cells. Toxicol Lett 378: 39-50, 2023.
14. Liudvytska O and Kolodziejczyk-Czepas J: A review on rhubarb-derived substances as modulators of cardiovascular risk factors-A special emphasis on anti-obesity action. Nutrients 14: 2053, 2022.
15. Qin MY, Huang SQ, Zou XQ, Zhong XB, Yang YF, Zhang YT, Mi ZC, Zhang YS and Huang ZG: Drug-containing serum of rhubarb-astragalus capsule inhibits the epithelial-mesenchymal transformation of HK-2 by downregulating TGF-beta1/p38MAPK/Smad2/3 pathway. J Ethnopharmacol 280: 114414, 2021.
16. Zou G, Zhang X, Wang L, Li X, Xie T, Zhao J, Yan J, Wang L, Ye H, Jiao S, *et al*: Herb-sourced emodin inhibits angiogenesis of breast cancer by targeting VEGFA transcription. Theranostics 10: 6839-6853, 2020.
17. Dai G, Wang D, Ma S, Hong S, Ding K, Tan X and Ju W: ACSL4 promotes colorectal cancer and is a potential therapeutic target of emodin. Phytomedicine 102: 154149, 2022.
18. Ma L, Chen K, Jiang K, Deng G, Jiang P, Shao J and Yu Z: Emodin inhibits the proliferation and invasion of bladder cancer cells by downregulatingating Notch1. Int J Clin Exp Pathol 10: 9452-9459, 2017.
19. Cha TL, Chuang MJ, Tang SH, Wu ST, Sun KH, Chen TT, Sun GH, Chang SY, Yu CP, Ho JY, *et al*: Emodin modulates epigenetic modifications and suppresses bladder carcinoma cell growth. Mol Carcinog 54: 167-177, 2015.
20. Luster MI, Tucker AN, Hayes HT, Pung OJ, Burka T, McMillan R and Eling T: Immunosuppressive effects of benzidine in mice: Evidence of alterations in arachidonic acid metabolism. J Immunol 135: 2754-2761, 1985.
21. Martin CN, Beland FA, Roth RW and Kadlubar FF: Covalent binding of benzidine and N-acetylbenzidine to DNA at the C-8 atom of deoxyguanosine in vivo and in vitro. Cancer Res 42: 2678-2686, 1982.
22. Wong HP, Ho JW, Koo MW, Yu L, Wu WK, Lam EK, Tai EK, Ko JK, Shin VY, Chu KM and Cho CH: Effects of adrenaline in human colon adenocarcinoma HT-29 cells. Life Sci 88: 1108-1112, 2011.
23. Fan X, Li J, Long L, Shi T, Liu D, Tan W, Zhang H, Wu X, Lei X and Wang Z: Design, synthesis and biological evaluation of N-anthraniloyl tryptamine derivatives as pleiotropic molecules for the therapy of malignant glioma. Eur J Med Chem 222: 113564, 2021.
24. Millerick-May ML, Wang L, Rice C and Rosenman KD: Ongoing risk of bladder cancer among former workers at the last benzidine manufacturing facility in the USA. Occup Environ Med 78: 625-631, 2021.
25. Letasiova S, Medve'ova A, Sovcikova A, Dušinská M, Volkovová K, Mosoiu C and Bartonová A: Bladder cancer, a review of the environmental risk factors. Environ Health 11 (Suppl 1): S11, 2012.
26. Sun X, Zhang T, Deng Q, Zhou Q, Sun X, Li E, Yu D and Zhong C: Benzidine induces epithelial-mesenchymal transition of human bladder cancer cells through activation of ERK5 pathway. Mol Cells 41: 188-197, 2018.
27. Soria F, Shariat SF, Lerner SP, Fritsche HM, Rink M, Kassouf W, Spiess PE, Lotan Y, Ye D, Fernández MI, *et al*: Epidemiology, diagnosis, preoperative evaluation and prognostic assessment of upper-tract urothelial carcinoma (UTUC). World J Urol 35: 379-387, 2017.

28. Farrow JM, Kern SQ, Gryzinski GM and Sundaram CP: Nephron-sparing management of upper tract urothelial carcinoma. Investig Clin Urol 62: 389-398, 2021.
29. Zhang FY, Li RZ, Xu C, Fan XX, Li JX, Meng WY, Wang XR, Liang TL, Guan XX, Pan HD, *et al*: Emodin induces apoptosis and suppresses non-small cell lung cancer growth via downregulation of sPLA2-IIa. Phytomedicine 95: 153786, 2022.
30. Akbari B, Soltantoyeh T, Shahosseini Z, Jadidi-Niaragh F, Hadjati J, Brown CE and Mirzaei HR: PGE2-EP2/EP4 signaling elicits mesoCAR T-cell immunosuppression in pancreatic cancer. Front Immunol 14: 1209572, 2023.
31. Kurtova AV, Xiao J, Mo Q, Pazhanisamy S, Krasnow R, Lerner SP, Chen F, Roh TT, Lay E, Ho PL and Chan KS: Blocking PGE2-induced tumor repopulation abrogates bladder cancer chemoresistance. Nature 517: 209-213, 2015.
32. Park MY, Kwon HJ and Sung MK: Evaluation of aloin and aloe-emodin as anti-inflammatory agents in aloe by using murine macrophages. Biosci Biotechnol Biochem 73: 828-832, 2009.
33. Hu H, Song X, Li Y, Ma T, Bai H, Zhao M, Wang X, Liu L and Gao L: Emodin protects knee joint cartilage in rats through anti-matrix degradation pathway: An in vitro and in vivo study. Life Sci 269: 119001, 2021.
34. Huang RY and Chen GG: Cigarette smoking, cyclooxygenase-2 pathway and cancer. Biochim Biophys Acta 1815: 158-169, 2011.
35. Wiktorowska-Owczarek A and Owczarek J: The effect of hypoxia on PGE2-stimulated cAMP generation in HMEC-1. Cell Mol Biol Lett 20: 213-221, 2015.
36. Ye Y, Wang X, Jeschke U and von Schönfeldt V: COX-2-PGE_2-EPs in gynecological cancers. Arch Gynecol Obstet 301: 1365-1375, 2020.
37. Li T, Hu J, Du S, Chen Y, Wang S and Wu Q: ERK1/2/COX-2/PGE2 signaling pathway mediates GPR91-dependent VEGF release in streptozotocin-induced diabetes. Mol Vis 20: 1109-1121, 2014.
38. Steinert D, Kuper C, Bartels H, Beck FX and Neuhofer W: PGE2 potentiates tonicity-induced COX-2 expression in renal medullary cells in a positive feedback loop involving EP2-cAMP-PKA signaling. Am J Physiol Cell Physiol 296: C75-C87, 2009.
39. Choudhary S, Kumar A, Kale RK, Raisz LG and Pilbeam CC: Extracellular calcium induces COX-2 in osteoblasts via a PKA pathway. Biochem Biophys Res Commun 322: 395-402, 2004.
40. Chen L, Sooranna SR, Lei K, Kandola M, Bennett PR, Liang Z, Grammatopoulos D and Johnson MR: Cyclic AMP increases COX-2 expression via mitogen-activated kinase in human myometrial cells. J Cell Mol Med 16: 1447-1460, 2012.